MOLECULAR AND CELLULAR BIOLOGY, June 2004, p. 5459–5474 Vol. 24, No. 12
0270-7306/04/$08.00+0 DOI: 10.1128/MCB.24.12.5459–5474.2004

Mitogen Stimulation Cooperates with Telomere Shortening To Activate DNA Damage Responses and Senescence Signaling

A. Satyanarayana,[1] R. A. Greenberg,[2] S. Schaetzlein,[1] J. Buer,[3,4] K. Masutomi,[5] W. C. Hahn,[5] S. Zimmermann,[6] U. Martens,[6] M. P. Manns,[1] and K. L. Rudolph[1]*

Department of Gastroenterology, Hepatology, and Endocrinology[1] and Department of Microbiology,[3] Medical School Hannover, Hannover, Department of Cell Biology, GBF, Braunschweig,[4] and Department of Hematology/Oncology, Medical University Center Freiburg, Freiburg,[6] Germany, and Department of Cancer Biology[2] and Department of Medical Oncology,[5] Dana Farber Cancer Institute, Boston, Massachusetts

Received 6 November 2003/Returned for modification 17 December 2003/Accepted 12 March 2004

Replicative senescence is induced by critical telomere shortening and limits the proliferation of primary cells to a finite number of divisions. To characterize the activity status of the replicative senescence program in the context of cell cycle activity, we analyzed the senescence phenotypes and signaling pathways in quiescent and growth-stimulated primary human fibroblasts in vitro and liver cells in vivo. This study shows that replicative senescence signaling operates at a low level in cells with shortened telomeres but becomes fully activated when cells are stimulated to enter the cell cycle. This study also shows that the dysfunctional telomeres and nontelomeric DNA lesions in senescent cells do not elicit a DNA damage signal unless the cells are induced to enter the cell cycle by mitogen stimulation. The amplification of senescence signaling and DNA damage responses by mitogen stimulation in cells with shortened telomeres is mediated in part through the MEK/mitogen-activated protein kinase pathway. These findings have implications for the further understanding of replicative senescence and analysis of its role in vivo.

Telomere shortening limits the growth of primary human cells to a finite number of cell divisions before proliferation ceases at the senescence stage (23). Cellular senescence induced by telomere shortening is characterized by typical changes in cell morphology (flattened cells with enlarged cytoplasm) (5, 23) and senescence-associated β-galactosidase (SA-β-Gal) activity at pH 6 (10). At the molecular level, growth arrest at the senescence stage is induced by an attenuation of gene expression and an accumulation of cells in the late G_1 phase of the cell cycle (13, 35, 37, 40) which fail to phosphorylate pRb after mitogen stimulation (50). Phosphorylation of pRb during G_1 phase is carried out by cyclin D-Cdk4/6 and cyclin E-Cdk2 complexes. This process is essential for the release of E2F transcription factors that promote the expression of late-G_1-phase genes that are required for S-phase initiation and progression (59). Once arrested, the senescent cells cannot be stimulated to enter S phase by any known combination of physiological mitogens. Many genes, including several proto-oncogenes, remain mitogen inducible in senescent cells (41, 47). Thus, senescent cells fail to proliferate not because of a loss of growth factor signal transduction but rather because of selective repression of a few positively acting, growth regulatory genes whose expression is essential for G_1-phase progression and DNA synthesis (41, 47).

It has been suggested that critically short telomeres at the cellular level determine whether a cell enters senescence or continues to divide both in vitro (3) and in vivo (44). A current hypothesis is that replicative senescence represents a DNA damage-like response induced by a loss of telomere function and chromosomal "uncapping" in cells with critically short telomeres (55). In accordance with this hypothesis, it was re-

TABLE 1. Primer pairs used for real-time quantitative PCR

Gene	Primer pair sequences
Mouse p21	5′-TTGTCGCTGTCTTGCACTCT-3′ 5′-AATCTGTCAGGCTGGTCTGC-3′
Mouse p16	5′-TCTGCTCAACTACGGTGCAG-3′ 5′-CACCAGCGTGTCCAGGAAG-3′
Mouse ARF	5′-GCTCTGGCTTTCGTGAACAT-3′ 5′-GTGAACGTTGCCCATCATC-3′
Human P21	5′-GCGACTGTGATGCGCTAAT-3′ 5′-GTCACCCTCCAGTGGTGTCT-3′
Human P16	5′-ACCAGAGGCAGTAACCATGC-3′ 5′-AAGTTTCCCGAGGTTTCTCA-3′
Human ARF	5′-CCAGGTGGGTAGAAGGTCTG-3′ 5′-GAGAATCGAAGCGCTACCTG-3′
Mouse RSP9	5′-CTGGACGAGGGCAAGATGAAGC-3′ 5′-TGACGTTGGCGGATGAGCACA-3′
Human β-actin	5′-GGACTTCGAGCAAGAGATGG-3′ 5′-AGGAAGGAAGGCTGGAAGAG-3′

* Corresponding author. Mailing address: Department of Gastroenterology, Hepatology, and Endocrinology, Medical School Hannover, Carl-Neuberg-Str. 1, 30625 Hannover, Germany. Phone: 0049-511-532-3489. Fax: 0049-511-532-2021. E-mail: Rudolph.Lenhard@Mh-Hannover.de.

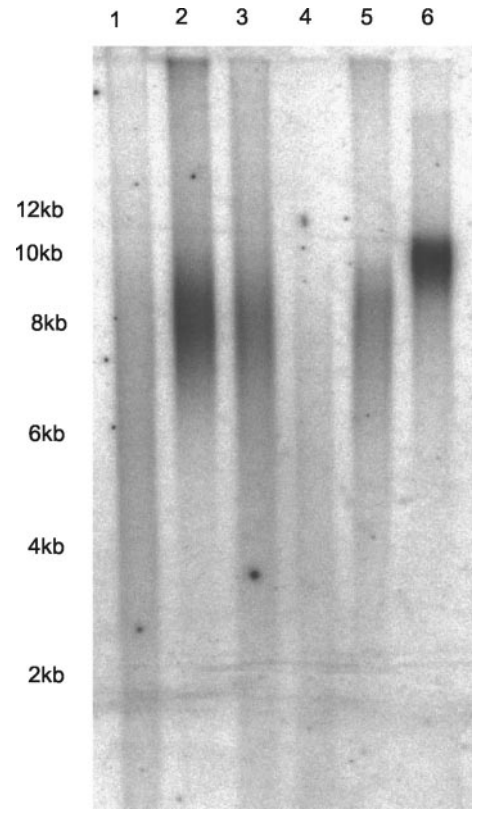

FIG. 1. TRF length determined for early-passage, late-passage, and hTERT-immortalized IMR90 and HK1 cells in a representative in-gel Southern blot. Lanes: 1, late-passage (PD55) IMR90 cells; 2, early-passage (PD30) IMR90 cells; 3, hTERT-immortalized (PD68) IMR90 cells; 4, late-passage (PD60) HK1 cells; 5, early-passage (PD9) HK1 cells; 6, hTERT-immortalized (PD90) HK1 cells. The mean TRF length was significantly shorter in late-passage IMR90 cells (5.7 kb) than in early-passage (8.5 kb) or hTERT-immortalized (7.8 kb) IMR90 cells. The mean TRF length was significantly shorter in late-passage HK1 cells (4.8 kb) than in early-passage (7.6 kb) or hTERT-immortalized (9.2 kb) HK1 cells.

cently shown that senescent cells are characterized by the appearance of nuclear DNA damage foci containing a variety of proteins involved in DNA damage checkpoint control and double-strand break repair (8, 45, 54). To a certain extent, these DNA damage foci localize to the dysfunctional telomeric ends (8, 54). It seems possible that the disruption of higher-order telomere structures, e.g., T loops (19) or G quartets (4), as well as the degradation of the G-strand overhang (31, 53) triggers this DNA damage response. However, there is also evidence for a genome-wide accumulation of nonrepairable double-strand breaks in senescent cells (45). In line with the DNA damage hypothesis of senescence, a variety of studies have revealed the activation of the p53-dependent up-regulation of the Cdk inhibitor $p21^{Cip1/Waf1/Sdi1}$ (7, 35, 44, 51) at senescence. In addition to the activation of the DNA damage response, the Cdk inhibitor $p16^{Ink4a}$ accumulates in senescent cell cultures (2, 20), and it has been proposed that it may be part of a differentiation program necessary for the maintenance of senescence (7).

Besides the induction of replicative senescence by critical telomere shortening, overstimulation of the Ras/Raf/MEK/mitogen-acrivated protein kinase (MAPK) pathway provokes premature senescence arrest irrespective of telomere length (29, 46, 62). Premature senescence induced by activated Ras and replicative senescence downstream of telomere shortening share common signaling pathways and morphological features (46). In primary human cells, the "premature senescence program" leads to the activation of p53 and p16 (29, 46), possibly functioning as a tumor suppressor mechanism (46). Another stress condition that has been linked to the activation of senescence programs includes oxidative stress and DNA damage (32). It has been demonstrated that oxidative stress can cooperate with telomere shortening to activate replicative senescence programs (57). Moreover, in mouse embryonal fibroblasts, oxidative stress appears to be the major mechanism for inducing senescence-like growth arrest (39). According to these studies, the activation of senescence may depend on multiple factors, including cellular stresses and telomere shortening. In line with this hypothesis, a recent study showed that in primary human fibroblasts, the activation of senescence during in vitro passage involves a mixture of different senescence stimuli, including oxidative and mitogenic stresses as well as telomere shortening (25). The interconnection among these different senescence stimuli has yet to be explored.

Our study focuses on the question of whether replicative senescence signaling is constitutively operative irrespective of external factors or modulated by altered mitogen stimulation that induces a proliferative response to drive the cells into the cell cycle. This study shows that replicative senescence signaling is amplified when cells with shortened telomeres are stimulated to enter the cell cycle by mitogens. The activation of senescence signaling correlates with the activation of DNA damage responses by mitogen stimulation. This study also

FIG. 2. The phenotype of replicative senescence of primary human fibroblasts is mitogen dependent. (A) Representative images of IMR90 cells at early passage and late passage, TERT-expressing IMR90 cells at late passage, and SV40-T-Ag-expressing IMR90 cells at late passage (rows from top to bottom) under the indicated culture conditions. (B and C) Histograms showing the percentage of cells with senescent morphology (B) and the percentage of SA-β-Gal-positive cells (C) for early-passage (PD30) and late-passage (PD55) IMR90 cells under serial passage in 10% FBS, after serum starvation in 0.1% FBS for 120 h, and after serum restimulation with 10% FBS for 24 h. The senescent morphology index and the number of SA-β-Gal-positive cells for early-passage IMR90 cells were low under all culture conditions. In contrast, late-passage IMR90 cells showed a high senescence morphology index (75.36% ± 6.14%) and a high percentage of SA-β-Gal-positive cells (78.34% ± 7.62%) under serial passage, a significant rescue of senescence morphology (23.43% ± 3.29%; $P < 0.0001$) and SA-β-Gal activity (19.29% ± 3.89%; $P < 0.0001$) in response to serum starvation, and a significant reappearance of senescence morphology (72.9% ± 8.17%; $P < 0.0001$) and SA-β-Gal activity (67.58% ± 8.86%; $P < 0.0001$) in response to serum restimulation. (D) Histogram showing the percentage of SA-β-Gal-positive cells for late-passage IMR90 cells expressing SV40-T-Ag (PD65) or hTERT (PD68) and showing no senescence phenotype irrespective of the culture conditions. Histogram data are presented as means and standard deviations.

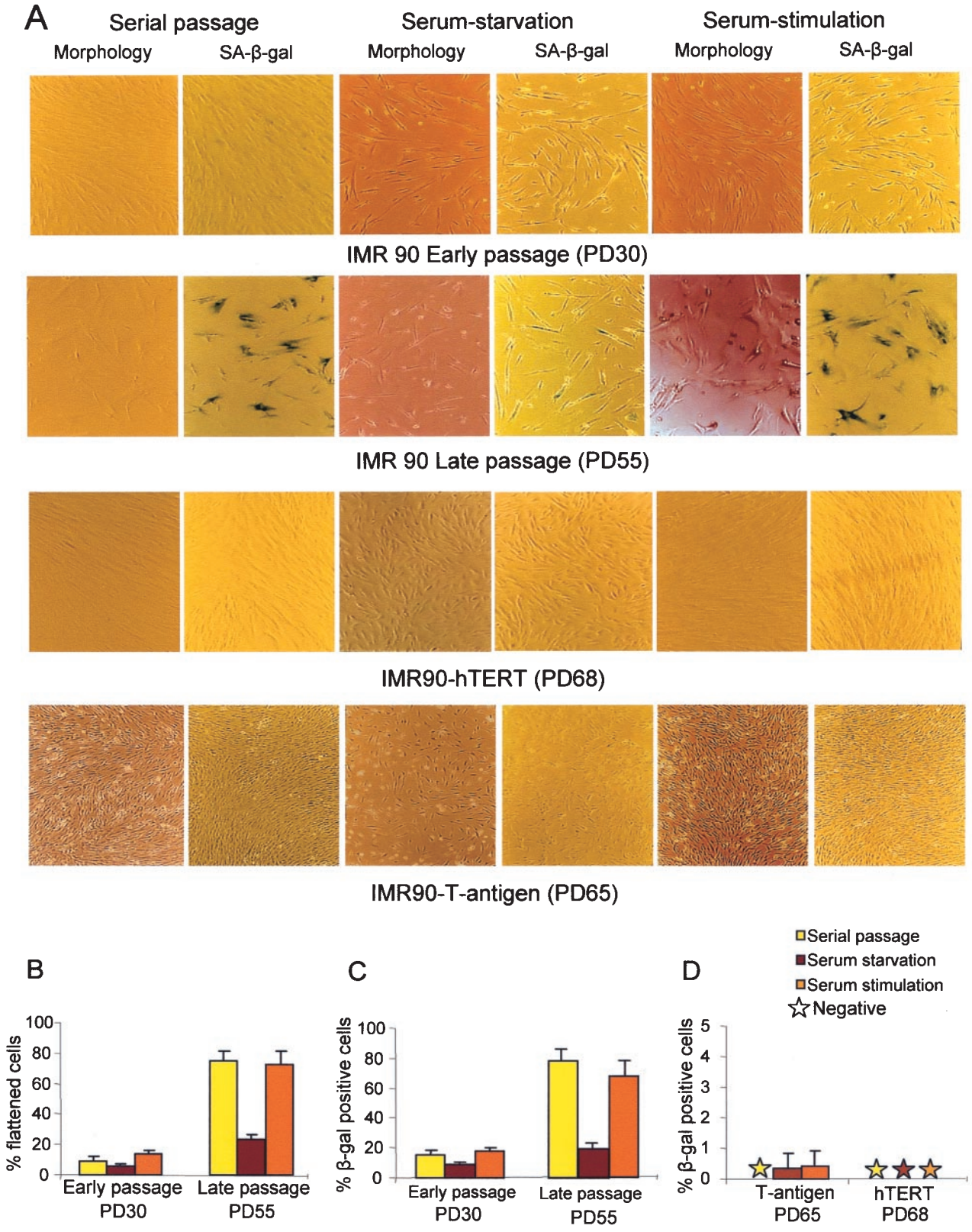
A
Serial passage
Serum-starvation
Serum-stimulation
Morphology
SA-β-gal
Morphology
SA-β-gal
Morphology
SA-β-gal
IMR 90 Early passage (PD30)
IMR 90 Late passage (PD55)
IMR90-hTERT (PD68)
IMR90-T-antigen (PD65)
B
% flattened cells
100
80
60
40
20
0
Early passage PD30
Late passage PD55
C
% β-gal positive cells
100
80
60
40
20
0
Early passage PD30
Late passage PD55
D
Serial passage
Serum starvation
Serum stimulation
Negative
% β-gal positive cells
5
4
3
2
1
0
T-antigen PD65
hTERT PD68

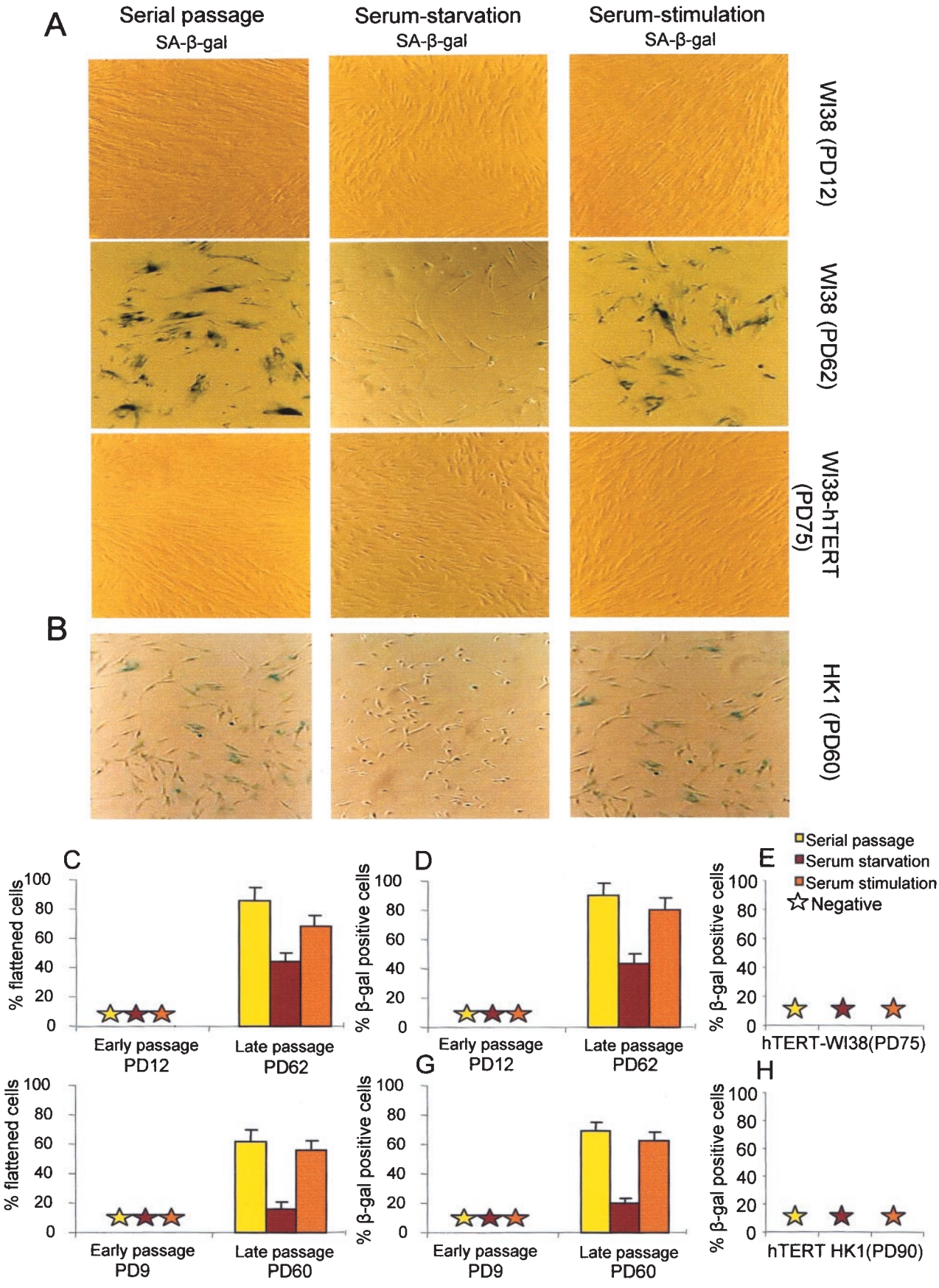
A
Serial passage
SA-β-gal
Serum-starvation
SA-β-gal
Serum-stimulation
SA-β-gal
WI38 (PD12)
WI38 (PD62)
WI38-hTERT (PD75)
B
HK1 (PD60)
C
% flattened cells
Early passage PD12
Late passage PD62
D
% β-gal positive cells
Early passage PD12
Late passage PD62
E
Serial passage
Serum starvation
Serum stimulation
Negative
% β-gal positive cells
hTERT-WI38(PD75)
% flattened cells
Early passage PD9
Late passage PD60
G
% β-gal positive cells
Early passage PD9
Late passage PD60
H
% β-gal positive cells
hTERT HK1(PD90)

shows that the activation of senescence signaling is mediated in part through the MEK/MAPK pathway.

MATERIALS AND METHODS

Cell cultures. Human fetal lung fibroblasts (IMR90), human embryo lung fibroblasts (WI38), and human adult skin fibroblasts (HK1) (62) were cultured in Dulbecco minimal essential medium (Gibco) supplemented with 10% fetal bovine serum (FBS) (Sigma) and 1% penicillin-streptomycin in 5% CO_2–20% O_2 at 37°C. Serum starvation was carried out with 0.1% FBS in DMEM for 120 h after trypsinization of serially passaged cultures. Serum restimulation was carried out with 10% FBS in DMEM. For drug (PD098059 or U0126) inhibition studies, cells were cultured in 0.1% FBS for 120 h and treated with a 10 μM final concentration of PD098059 or U0126 1 h before serum stimulation.

Flattened cells were defined as exceeding 60 μm in width, and their shape thus was clearly distinguishable from the normal spindle-like shape of the majority of fibroblasts at early passage, having a width of 20 to 40 μm. The number of flattened cells in cultures of living cells under serial passage, serum starvation, and serum stimulation conditions and in response to drug treatment (see above) was counted directly by using a microscope. For each culture condition, the cells were counted in at least 10 low-power fields (×10). Then, the cells were washed twice with phosphate-buffered saline (PBS), fixed with 10% formalin in PBS for 10 min, washed three times with PBS, and stained with crystal violet staining solution (50 mg of crystal violet, 45 ml of H_2O, 5 ml of ethanol) for 30 min. The excess stain was removed by washing the cells with distilled H_2O five to seven times. The plates then were air dried, and the number of irregular, flattened cells in a minimum of 10 low-power fields (×10) was counted again and expressed as a percentage of all cells counted. Similar results were obtained with the above two counting methods.

Cell cycle profile. Cells were pulse-labeled with bromodeoxyuridine (BrdU) at a 10 μM final concentration for 2 h before collection and stained with propidium iodide and fluorescein isothiocyanate (FITC)-labeled anti-BrdU antibody (Becton Dickinson) according to the manufacturer's protocol. Flow cytometric analysis was carried out with a FACScan apparatus (Becton Dickinson) equipped with Cellquest software.

TRF length analysis. Telomere restriction fragment (TRF) length analysis of genomic DNA collected from early-passage, late-passage, and human TERT (hTERT)-immortalized primary human fibroblasts was done as described previously (60).

Mice. Two- to 3-month-old male $mTERC^{-/-}$ and littermate $mTERC^{+/+}$ control mice in a C57BL/6J background were used for this study. Late-generation $mTERC^{-/-}$ mice were obtained by crossing successive generations of $mTERC^{-/-}$ mice until the third generation (G_3). The mice were bred and maintained on a standard diet in the animal facility at Medical School Hannover.

PH and BrdU pulse-labeling. All of the mice underwent 70% partial hepatectomy (PH) in the early hours of the day. The mice were pulse-labeled with BrdU by intraperitoneal injection of BrdU labeling reagent (10 μl/g of body weight; cell proliferation kit; Amersham) 2 h before sacrifice. Immunohistochemical staining of frozen sections was done as described before (44).

SA-β-Gal staining. SA-β-Gal staining was carried out as described previously (10) with cryostat sections of liver samples collected 24 to 120 h after PH. Cells were stained after fixation in 3% formaldehyde for 5 min with freshly prepared SA-β-Gal solution overnight at 37°C in the dark. Five independent stainings were carried out for both early- and late-passage cells. Analysis was done in a blinded fashion. The number of SA-β-Gal-positive cells in 10 low-power fields (×10) was counted randomly and expressed as a percentage of all cells counted.

Determination of IL-6 levels. Serum interleukin 6 (IL-6) levels in blood serum were determined by using a Pharmingen OptEIA set mouse IL-6 kit according to the manufacturer's protocol.

Q-FISH. Quantitative fluorescent in situ hybridization (Q-FISH) to measure telomere lengths was conducted with liver cells isolated from $mTERC^{+/+}$ and G_3 $mTERC^{-/-}$ mice by the collagenase perfusion method (44) as described before (60).

RNA extraction and cDNA synthesis. Total RNA was extracted from liver samples and from early-passage, late-passage, hTERT-immortalized, and drug-treated fibroblasts by using RNA Clean according to the manufacturer's protocol (Hybaid). The RNA was extracted from liver samples collected 36 h ($n = 3$) after PH and from mice that did not undergo hepatectomy ($n = 5$) in each group ($mTERC^{+/+}$ and G_3 $mTERC^{-/-}$). The quality of the RNA was checked on a denaturing agarose gel, and the concentration was determined by using a spectrophotometer at 260 nm (optical density at 260 nm [OD_{260}]). RNA samples having an OD_{260}/OD_{280} ratio of 2 or more were used for cDNA synthesis and quantitative real-time PCR. A total of 2 μg of total RNA was used to synthesize cDNA with an oligo-dT primer and Superscript II reverse transcriptase (RT) enzyme (Invitrogen). The RT reaction was checked by amplifying the RSP9 and β-actin housekeeping genes.

Quantitative real-time PCR. Quantitative real-time PCR was performed by using an ABI Prism 7700 sequence detection system (PE Applied Biosystems) with SYBR green I (Sigma S9430) as a double-stranded DNA-specific binding dye. All of the samples were analyzed in triplicate, and expression was confirmed by three independent PCR runs. The primer pairs used are listed in Table 1. The cycle profile for PCR was as follows. After activation of Hot Star Taq DNA polymerase (Qiagen), denaturation was carried out at 94°C for 15 s, annealing was carried out at 54°C for 15 s, and extension was carried out at 72°C for 30 s. A total of 45 cycles of PCR amplification were performed to confirm the expression level; to normalize the expression level, the internal controls used were the RSP9 housekeeping gene for mouse liver and the β-actin housekeeping gene for primary human fibroblasts. The optimum temperature for the analysis of a specific product was obtained after amplification by raising the temperature successively through 0.5°C steps and comparing the melting temperature of a specific product with that of a nonspecific product. The optimum temperature determined from melting point analysis then was used for quantitative PCR. The quantification data were analyzed with ABI Prism 7700 analysis software. In all experiments, the value used to determine the cycle threshold during analysis was kept constant. For each primer pair, the linearity of detection was confirmed to obtain a correlation coefficient of at least 0.98 over the detection area by measuring a fourfold dilution curve with cDNA prepared from liver samples and from IMR90 and HK1 cells. The fold difference therefore was calculated by assuming a 100% efficient PCR where each cycle threshold was normalized to the expression of the RSP9 or β-actin housekeeping gene. The results are reported as means and standard deviations for three different PCRs.

Immunocytochemical analysis. Early-passage and late-passage HK1 cells were grown on coverslips and probed with specific antibodies during serial passage, serum starvation (0.1% FBS for 120 h), restimulation (10% FBS for 24 h), and

FIG. 3. (A) Representative images of SA-β-Gal activity for early-passage (PD12), late-passage (PD62), and late-passage hTERT-expressing (PD75) WI38 cells. (B) Representative images of SA-β-Gal activity for late-passage (PD60) HK1 cells. (C and D) Histograms showing the percentages of WI38 cells with senescent morphology (C) and SA-β-Gal activity (D) for early-passage (PD12) and late-passage (PD62) cells under serial passage in 10% FBS, in response to serum starvation in 0.1% FBS for 120 h, and in response to serum restimulation with 10% FBS for 24 h. Under serial passage, late-passage WI38 cells showed high rates of senescent morphology (85.62% ± 9.69%) and SA-β-Gal activity (89.8% ± 8.16%). Both markers were rescued in response to serum starvation (44.27% ± 5.52% for senescence morphology [$P < 0.0001$] and 43.2% ± 6.56% for SA-β-Gal activity [$P < 0.0001$]) but reappeared in response to serum restimulation (68.06% ± 8.19% for senescence morphology [$P < 0.0001$] and 79.69% ± 9.05% for SA-β-Gal activity [$P < 0.0001$]). (E) Histogram showing the absence of SA-β-Gal-positive cells for late-passage hTERT-expressing (PD75) WI38 cells in response to three different culture conditions. (F and G) Histograms showing the percentages of HK1 cells with senescent morphology (F) and SA-β-Gal activity (G) for early-passage (PD9) and late-passage (PD60) cells under serial passage in 10% FBS, in response to serum starvation in 0.1% FBS for 120 h, and in response to serum restimulation in 10% FBS. Under serial passage, late-passage HK1 cells showed high rates of senescent morphology (61.73% ± 5.27%) and SA-β-Gal activity (68.93% ± 6.11%). Both markers were rescued in response to serum starvation (15.98% ± 4.47% for senescence morphology [$P < 0.0001$] and 19.89% ± 3.42% for SA-β-Gal activity [$P < 0.0001$]) but reappeared in response to serum restimulation (55.76% ± 6.73% for senescence morphology [$P < 0.0001$] and 62.68% ± 5.59% for SA-β-Gal activity [$P < 0.0001$]). (H) Histogram showing the absence of SA-β-Gal-positive cells for late-passage hTERT-expressing (PD90) HK1 cells in response to three different culture conditions. Histogram data are presented as means and standard deviations.

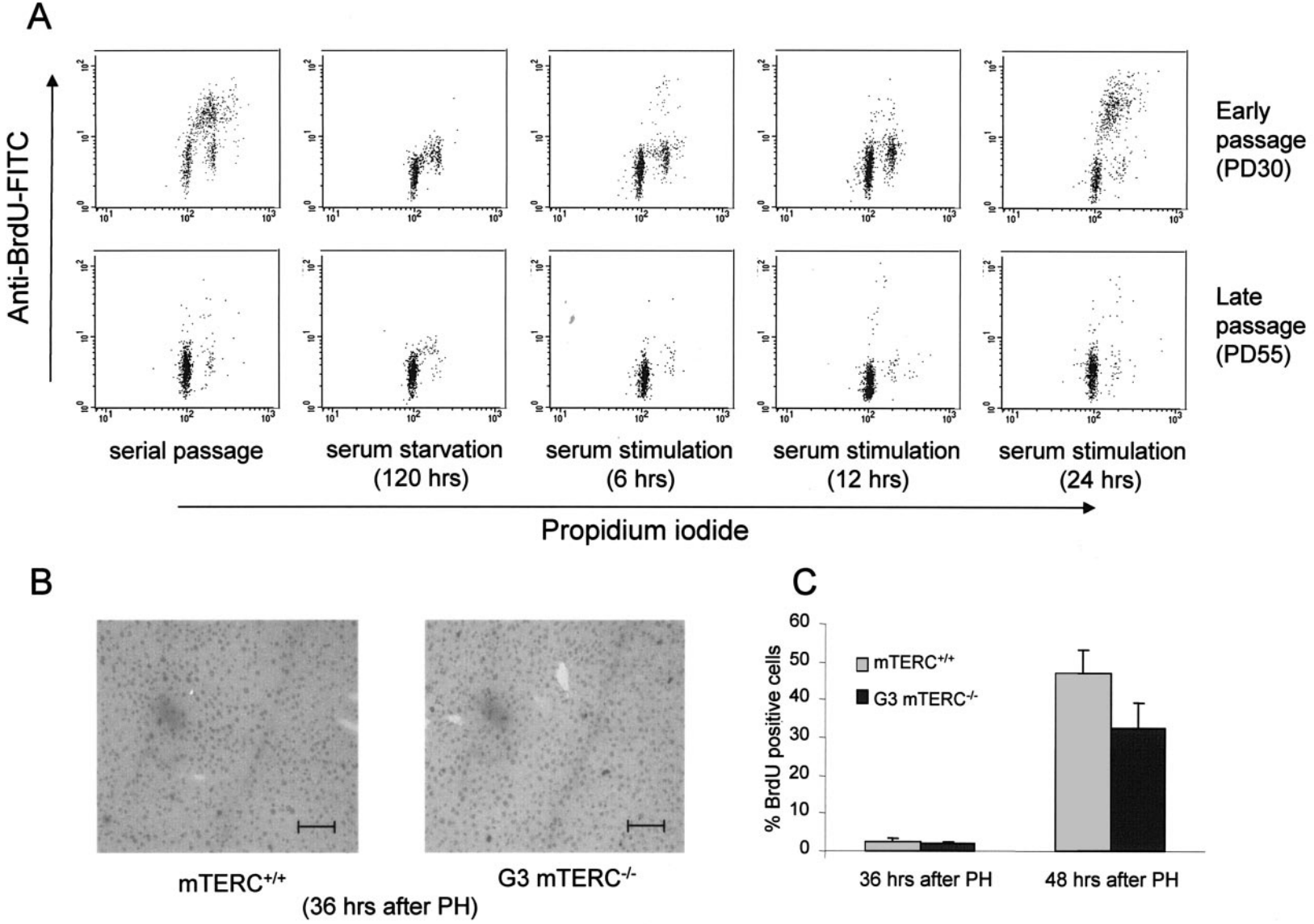

FIG. 4. Impaired cell cycle activity and accumulation of cells in G_1 phase of the cell cycle during late passage. (A) Representative data from one of three independent flow cytometric analyses of early- and late-passage IMR90 cells under the indicated culture conditions. About 90% of the late-passage cells accumulated in G_1 phase of the cell cycle even after 24 h of serum stimulation. (B) Representative BrdU staining patterns at the onset of S phase (36 h after PH) in mTERC$^{+/+}$ and G_3 mTERC$^{-/-}$ mice. Bar, 150 μm. (C) Percentages of BrdU-positive cells for mTERC$^{+/+}$ and G3 mTERC$^{-/-}$ mice at 36 h (2.3% ± 1.08% versus 1.75% ± 0.77%) and 48 h (44.03% ± 6.33% versus 32.31% ± 6.65%) after PH, as determined by 2 h of BrdU pulse-labeling. Data are presented as means and standard deviations.

TABLE 2. Cell cycle profiles for early- and late-passage IMR90 and HK1 cells at various times and culture conditions

Cells[a]	Culture condition	Mean ± SD % of cells in:					
		Early passage			Late passage		
		G_1	S	G_2/M	G_1	S	G_2/M
IMR90	Serial passage	38.6 ± 1.0	45.6 ± 1.7	15.6 ± 2.8	89.6 ± 6.0	5.2 ± 1.0	5.52 ± 0.3
	Starvation (120 h)	89.8 ± 2.5	0.83 ± 0.6	9.3 ± 1.9	97.7 ± 2.2	0.06 ± .05	2.17 ± 0.2
	Stimulation (6 h)	81.4 ± 2.0	4.2 ± 0.3	14.2 ± 1.8	96.1 ± 5.1	1.0 ± 0.5	3.1 ± 0.1
	Stimulation (12 h)	72.0 ± 2.3	9.1 ± 1.6	18.8 ± 0.7	92.3 ± 2.4	3.81 ± 0.4	3.87 ± 0.7
	Stimulation (24 h)	31.7 ± 3.2	60.5 ± 2.1	7.6 ± 1.8	87.6 ± 4.9	7.0 ± 0.7	5.35 ± 0.4
HK1	Serial passage	35.4 ± 2.2	53.0 ± 0.2	11.5 ± 2.1	81.7 ± 1	11.2 ± 1.7	6.92 ± 1.3
	Starvation (120 h)	90.7 ± 0.4	0.93 ± 0.2	8.3 ± 0.5	97.0 ± 2.0	0.0 ± 0.0	2.90 ± 2.0
	Stimulation (6 h)	86.2 ± 1.5	3.51 ± 0.5	9.92 ± 0.9	95.3 ± 1.4	1.0 ± 0.7	3.68 ± 0.7
	Stimulation (12 h)	73.9 ± 2.2	8.54 ± 1.4	17.5 ± 0.9	87.5 ± 3.8	6.34 ± 1.9	6.03 ± 1.9
	Stimulation (24 h)	30.4 ± 4.0	61.6 ± 6.4	7.6 ± 2.1	78.5 ± 4.6	13.0 ± 2.7	8.36 ± 1.9

[a] Early passages for IMR90 and HK1 cells were PD30 and PD9, respectively. Late passages for IMR90 and HK1 cells were PD55 and PD60, respectively.

treatment with MEK inhibitor U0126 (10 μM) before serum stimulation. The cells were washed twice with cold PBS, fixed either with ice-cold acetone-methanol (1:1) for 5 min or with 2% paraformaldehyde for 10 min, and washed three times with ice-cold PBS. The cells were permeabilized with 0.5% NP-40, washed three times with ice-cold PBS, and incubated with specific primary antibodies (2 μg/ml, except for MDC1, which was used at a 1:500 dilution) at 4°C overnight. The following primary antibodies were used for immunocytochemical analysis: anti-phospho-H2A.X (Ser139) and anti-53BP1 (Upstate), phospho-(Ser/Thr) ATM/ATR substrate (Cell Signaling), MDC1 (a kind gift from Stephen P. Jackson, University of Cambridge, Cambridge, England), and NBS1 (Oncogene). The cells were washed three times with PBS, incubated with FITC- or CY_3-conjugated secondary antibodies (Jackson Immunoresearch Laboratories) for 30 min at room temperature, and washed three times with PBS. The coverslips were air dried for 10 min and mounted with 4′,6′-diamidino-2-phenylindole mounting medium. A minimum of at least 500 nuclei in several low-power fields (×40) were counted randomly for each culture condition and for each antibody staining and were expressed as a percentage of all nuclei counted.

Statistical programs. Student's *t* test, Graphpad InStat, and Graphpad Prism software was used to calculate statistical significance and standard deviations.

RESULTS

The in vitro phenotype of replicative senescence induced by telomere shortening is dependent on mitogen stimulation. To analyze whether the senescence phenotype induced by telomere shortening is constitutively operative at the same level or is amplified by mitogenic stimuli, we first explored this phenomenon in human fibroblast cultures with three different cell lines (IMR90, WI38, and HK1) (27, 36, 56). As described in previous studies, telomeres were significantly shorter in late-passage cells of all three cell lines than in early-passage cells, but telomere length was stabilized by the overexpression of TERT (Fig. 1; data not shown for WI38 cells) (21, 27, 34, 36, 56).

Decreased cell proliferation at the onset of senescence correlated with an increased prevalence of the markers of cellular senescence: (i) SA-β-Gal activity at pH 6 and (ii) senescence cell morphology (flattened, irregular cells with an enlarged cytoplasm and a width of >60 μm). Consistent with previous studies, the percentage of cells that were positive for both markers reached >60% at late passage, whereas it was <20% at early passage (Fig. 2 and 3). To test whether these markers of replicative senescence were modulated by altered mitogen stimuli, their prevalence in early- and late-passage cells was quantitated (i) under serial passage, (ii) after serum starvation (0.1% FBS for 120 h), and (iii) after serum restimulation (10% FBS for 24 h). Interestingly, these experiments revealed that the increase in the percentage of cells showing senescence morphology or positive SA-β-Gal staining at late passage was strongly dependent on serum stimulation but almost completely disappeared in response to serum starvation (Fig. 2 and 3). The diminution of senescence markers in late-passage cultures was detectable as early as 48 h after serum starvation (data not shown) and reappeared 24 h after serum stimulation.

To ensure that the phenotype of senescence in late-passage fibroblasts was induced by telomere shortening, we performed an identical experiment with immortalized subclones of all three cell lines, in which replicative senescence was bypassed by hTERT expression. The immortalization of WI38 by hTERT expression was documented in an earlier study (27); similarly, hTERT expression was found to be sufficient to immortalize HK1 cells (63). There is some conflict on the immortalization of IMR90 cells; however, under our laboratory conditions, we successfully established IMR90 cells in which the replicative senescence limit clearly was bypassed by hTERT overexpression (the cells were monitored until population doubling 115 [PD115]), in line with observations made by others (34; J. Shay, personal communication). It has been reported that even though TERT expression elongates the life span of IMR90 cells, they still reach telomere-independent senescent arrest at very late passage (34). We cannot exclude the possibility that such telomere-independent factors also have a role in our in vitro experiments with IMR90 cells. However, the presence of similar findings in three different cell lines favors the conclusion that our experiments are in fact generally relevant for replicative senescence which is induced by telomere shortening and which can be bypassed by hTERT expression.

All three immortalized cell lines showed telomere stabilization after hTERT expression (Fig. 1; data not shown for WI38 cells) and no detectable senescence morphology or SA-β-Gal staining in late-passage cells independent of the culture conditions (Fig. 2A and D and Fig. 3A, E, and H). Similarly, simian virus 40 T antigen (SV40-T-Ag) expression, which blocks both the pRb and the p53 pathways, which govern the senes-

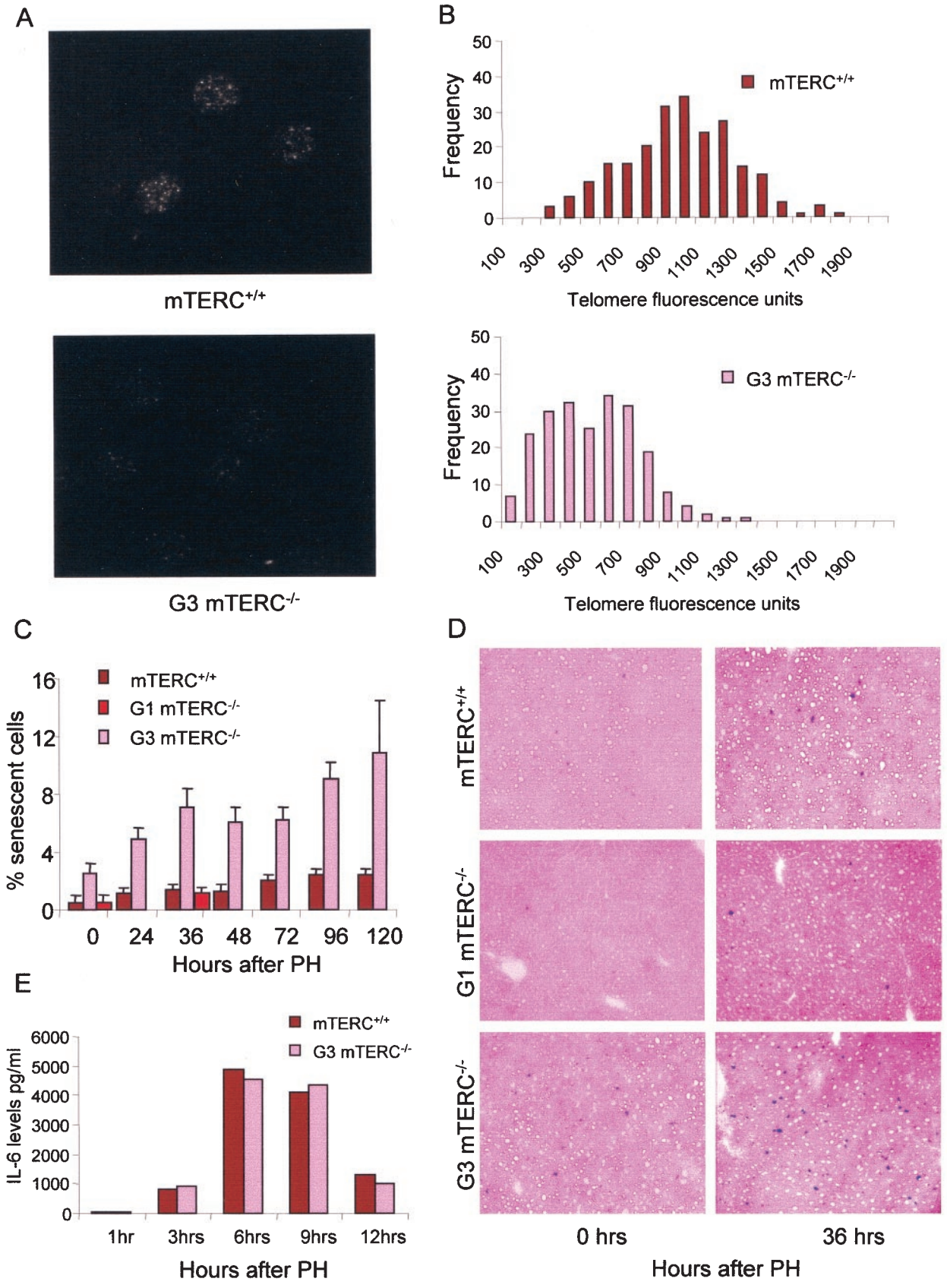
A
mTERC+/+
G3 mTERC-/-
B
Frequency
mTERC+/+
Telomere fluorescence units
G3 mTERC-/-
C
% senescent cells
mTERC+/+
G1 mTERC-/-
G3 mTERC-/-
Hours after PH
D
mTERC+/+
G1 mTERC-/-
G3 mTERC-/-
0 hrs
36 hrs
Hours after PH
E
IL-6 levels pg/ml
mTERC+/+
G3 mTERC-/-
1hr
3hrs
6hrs
9hrs
12hrs
Hours after PH

cence checkpoint (61), prevented the induction of senescence morphology and SA-β-Gal activity in late-passage IMR90 cells (Fig. 2A and D). Together, these data indicated that the classical senescence phenotype (induced by telomere shortening and bypassed by hTERT or SV40-T-Ag expression) in primary human cells can be modulated by altered mitogen stimulation. To rule out the possibility that further telomere shortening in subsequent cell division was the cause for this increased senescence phenotype in response to mitogen stimulation, we analyzed S-phase activity in IMR90 and HK1 cells. Early-passage cells showed S-phase activity under serial passage and resumption of replication 12 to 24 h after serum stimulation of serum-starved cultures. In contrast, late-passage fibroblasts did not show any significant S-phase activity under serial passage or after serum stimulation of serum-starved cultures (Fig. 4A and Table 2). These data excluded the possibility that the reappearance of the senescence phenotype in response to serum stimulation of late-passage human fibroblast cultures was due to further telomere shortening in subsequent cell division.

SA-β-Gal activity induced by telomere shortening in vivo is mitogen dependent. Several reports of studies with human samples have shown an increased frequency of SA-β-Gal-positive cells in organs and tissues affected by telomere shortening due to continuous cell turnover during aging (5, 10) or chronic diseases (38, 60). Late-generation telomerase-deficient mice ($mTERC^{-/-}$) have been used as a model system to study the impact of telomere shortening in vivo (6, 24, 28, 42, 43). It was recently reported that regenerative defects in late-generation $mTERC^{-/-}$ mice are in part due to the induction of cellular senescence and the failure to enter the cell cycle in a subpopulation of organ cells harboring critically short telomeres (44).

To test whether our in vitro result of mitogen-dependent alteration of the replicative senescence phenotype would also apply to the in vivo situation, we monitored SA-β-Gal activity in quiescent liver and liver stimulated to divide by PH in $mTERC^{-/-}$ and $mTERC^{+/+}$ mice. We used $mTERC^{-/-}$ mice of the first generation (G_1), which lack telomerase activity but have long telomere reserves and no apparent phenotype (6), as well as G_3 $mTERC^{-/-}$ mice, which have critically short telomeres (Fig. 5A and B). The quiescent liver has very little mitotic activity, with over 95% of the cells in the G_0 phase of the cell cycle; however, in response to pH, over 90% of liver cells participate in organ regeneration and restore organ mass within 1 week (15). As reported previously, there was an overall higher prevalence of SA-β-Gal-positive liver cells in G_3 $mTERC^{-/-}$ mice, harboring critically short telomeres, than in $mTERC^{+/+}$ mice (44). Similar to our in vitro data, the increased incidence of SA-β-Gal-positive cells in G_3 $mTERC^{-/-}$ mice was mitogen dependent, showing a strong increase after PH (Fig. 5C and D). In contrast, $mTERC^{+/+}$ and G_1 $mTERC^{-/-}$ mice showed only a slight increase in SA-β-Gal-positive cells, indicating that the induction of SA-β-Gal activity in vivo depends on both telomere shortening and mitogen stimulation. The increase in SA-β-Gal-positive liver cells in G_3 $mTERC^{-/-}$ mice after PH followed an increase in the levels in serum of IL-6—the prominent mitogen regulating liver cell cycle reentry in response to organ damage—and there was no difference in the mitogenic responses of $mTERC^{+/+}$ and G_3 $mTERC^{-/-}$ mice (Fig. 5E). Analysis of S-phase activity showed almost zero activity at 36 h but a sharp peak at 48 h after PH (Fig. 4B and C), indicating that the senescence phenotype in G_3 $mTERC^{-/-}$ liver, which became detectable at 36 h after PH, was independent of further telomere attrition in subsequent cell division.

The enhanced expression of cell cycle inhibitors induced by telomere shortening is mitogen dependent. To monitor molecular markers of replicative senescence, we monitored gene expression levels for cell cycle inhibitors regulating the senescence pathway, namely, p21 and p16 (2, 7, 20, 35, 51), and for $p19^{ARF}$, although its role in senescence is under debate (11, 58). As established in previous studies, increased expression of p21 was detected in late-passage cells (Fig. 6E, F, G, and J) (7, 35, 51) and in the regenerating liver of G_3 $mTERC^{-/-}$ mice compared to $mTERC^{+/+}$ and G_1 $mTERC^{-/-}$ mice (Fig. 6A and D) (44). Similarly, up-regulation of p16 was seen in late-passage cells (Fig. 6E, F, H, and K) (2, 20) but not in the regenerating liver of G_3 $mTERC^{-/-}$ mice (Fig. 6B), in line with previously identified species differences in the regulation of p16 during senescence in mouse and human cells (49). We did not detect significant up-regulation of $p19^{ARF}$ in either the in vitro or the in vivo system (Fig. 6C, I, and L).

In accordance with our data on senescence morphology and SA-β-Gal-activity, the senescence-associated up-regulation of p21 in late-passage cells and G_3 $mTERC^{-/-}$ mouse liver and the up-regulation of p16 in late-passage cells were strongly induced when the cells were stimulated to enter the cell cycle by mitogen exposure (Fig. 6A, D, E to H, J, and K). Moreover, mitogen withdrawal reversed the up-regulation of these Cdk inhibitors to a low, basal level when senescent late-passage cells were transferred from serial passage in 10% FBS to serum starvation in 0.1% FBS (Fig. 6E to H, J, and K). With the liver system, it has been reported that p21 is induced during cell cycle reentry of quiescent hepatocytes following PH (1), indi-

FIG. 5. The prevalence of SA-β-Gal staining in response to telomere shortening in vivo is mitogen dependent. (A) Representative images of Q-FISH analysis of interphase nuclei of liver cells obtained from $mTERC^{+/+}$ and G_3 $mTERC^{-/-}$ mice and hybridized with telomere-specific probe CY_3-OO-$(CCCTAA)_3$. (B) Histograms showing the distributions of mean telomere fluorescence intensities in nuclei of liver cells from G_3 $mTERC^{-/-}$ mice ($n = 3$) and $mTERC^{+/+}$ mice ($n = 3$). The data show significantly lower overall mean intensities in G_3 $mTERC^{-/-}$ mice than in $mTERC^{+/+}$ mice (565 ± 83.17 versus 1,027 ± 135.23 [$P < 0.0001$]). (C) Histograms showing the percentages of SA-β-Gal-positive cells in quiescent and regenerating liver cells from $mTERC^{+/+}$, G_1 $mTERC^{-/-}$, and G_3 $mTERC^{-/-}$ mice. Data are presented as means and standard deviations and show a significant increase in the percentage of SA-β-Gal-positive cells in G_3 $mTERC^{-/-}$ liver after PH but not in $mTERC^{+/+}$ liver. Note that SA-β-Gal staining was analyzed only in quiescent livers and 36 h after PH for G_1 $mTERC^{-/-}$ mice, and the values were comparable to those for $mTERC^{+/+}$ mice. (D) Representative images of SA-β-Gal staining of liver samples from $mTERC^{+/+}$, G_1 $mTERC^{-/-}$, and G_3 $mTERC^{-/-}$ mice at the quiescence stage and 36 h after PH. (E) Histogram showing similar IL-6 levels in the sera of $mTERC^{+/+}$ and G_3 $mTERC^{-/-}$ mice after PH; these levels peaked 6 to 9 h after PH.

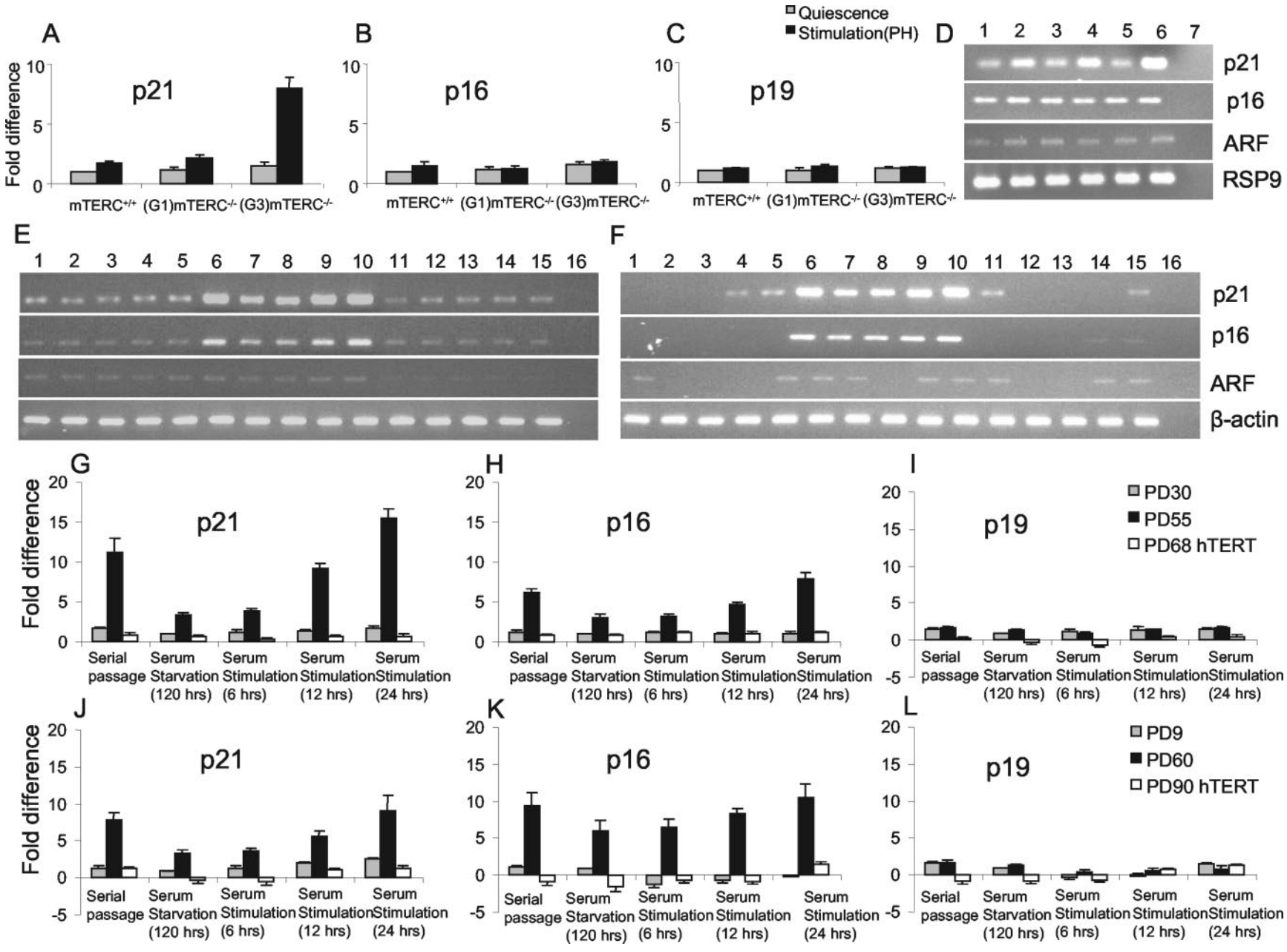
A
p21
Fold difference
mTERC+/+ (G1)mTERC-/- (G3)mTERC-/-
B
p16
C
p19
Quiescence
Stimulation(PH)
D
1 2 3 4 5 6 7
p21
p16
ARF
RSP9
E
1 2 3 4 5 6 7 8 9 10 11 12 13 14 15 16
F
1 2 3 4 5 6 7 8 9 10 11 12 13 14 15 16
p21
p16
ARF
β-actin
G
p21
Fold difference
H
p16
I
p19
PD30
PD55
PD68 hTERT
Serial passage
Serum Starvation (120 hrs)
Serum Stimulation (6 hrs)
Serum Stimulation (12 hrs)
Serum Stimulation (24 hrs)
J
p21
Fold difference
K
p16
L
p19
PD9
PD60
PD90 hTERT

FIG. 6. The enhanced expression of cell cycle inhibitors associated with replicative senescence in response to telomere shortening is mitogen dependent. (A to C) Histograms at the level of mRNA expression for p21 (A), p16 (B), and $p19^{ARF}$ (C) in quiescent liver and regenerating liver (36 h after PH) of $mTERC^{+/+}$, G_1 $mTERC^{-/-}$, and G3 $mTERC^{-/-}$ mice, as revealed by RT-PCR. While p16 and $p19^{ARF}$ showed no significant regulation, p21 was significantly overexpressed in G_3 $mTERC^{-/-}$ mice in response to PH (8-fold ± 0.88-fold up-regulation compared to the regulation in $mTERC^{+/+}$ quiescent liver) but not in the quiescent organ. (D) Representative gel electrophoresis image showing the RT-PCR products for p21, p16, and $p19^{ARF}$ (after 22 cycles) and the RSP9 housekeeping gene (after 35 cycles). Lanes: 1, quiescent $mTERC^{+/+}$ liver; 2, $mTERC^{+/+}$ liver 30 to 36 h after PH; 3, quiescent G_1 $mTERC^{-/-}$ liver; 4, G_1 $mTERC^{-/-}$ liver 30 to 36 h after PH; lane 5, quiescent G_3 $mTERC^{-/-}$ liver; 6, G_3 $mTERC^{-/-}$ liver 30 to 36 h after PH; 7, nontemplate control. (E) Representative gel electrophoresis image showing the levels of expression of p21, p16, and $p19^{ARF}$ (after 22 cycles) and the β-actin housekeeping gene (after 30 cycles) in IMR90 cells in the following loading order (lanes): 1 to 5, early-passage (PD30) IMR90 cells during serial passage (lane 1), serum starvation for 120 h (lane 2), serum stimulation for 6 h (lane 3), serum stimulation for 12 h (lane 4), and serum stimulation for 24 h (lane 5); 6 to 10, late-passage (PD55) IMR90 cells during serial passage (lane 6), serum starvation for 120 h (lane 7), serum stimulation for 6 h (lane 8), serum stimulation for 12 h (lane 9), and serum stimulation for 24 h (lane 10); 11 to 15, late-passage hTERT-expressing (PD68) IMR90 cells during serial passage (lane 11), serum starvation for 120 h (lane 12), serum stimulation for 6 h (lane 13), serum stimulation for 12 h (lane 14), and serum stimulation for 24 h (lane 15); 16, nontemplate control. (F) Representative gel electrophoresis image showing the levels of expression of p21, p16, and $p19^{ARF}$ (after 22 cycles) and the β-actin housekeeping gene (after 30 cycles) in HK1 cells. The loading of PCR products for early-passage (PD9), late-passage (PD60), and hTERT-immortalized (PD90) HK1 cells followed the same order as that described for IMR90 cells. (G to I) Histograms showing p21 (G), p16 (H), and $p19^{ARF}$ (I) expression in early- and late-passage IMR90 cells and in late-passage hTERT-expressing IMR90 cells. p21 and p16 were significantly up-regulated in late-passage IMR90 cells but not in hTERT-expressing cells. Note that serum starvation rescued the overexpression of p21 and p16, which reappeared 12 to 24 h after serum restimulation. (J to L) Histograms showing p21 (J), p16 (K), and $p19^{ARF}$ (L) expression in early- and late-passage HK1 cells and in late-passage HK1 cells expressing hTERT. p21 and p16 were significantly up-regulated in late-passage HK1 cells but not in hTERT-expressing cells. Note that serum starvation partially rescued the overexpression of p16 and nearly completely rescued the overexpression of p21, which reappeared 12 to 24 h after serum restimulation. Histogram data are presented as means and standard deviations.

cating that it plays a role in regulating cell cycle reentry during liver regeneration. However, the up-regulation of p21 in G_3 $mTERC^{-/-}$ mice in response to PH greatly exceeded the physiological up-regulation of p21 in wild-type or G_1 $mTERC^{-/-}$ mice (Fig. 6A and D).

The accumulation of DNA damage response proteins in cells with shortened telomeres is mitogen dependent. The cellular response to DNA damage usually starts with the sensing of the damaged DNA. ATM/ATR kinases are emerging as potential sensors whose induction leads to the activation by phosphorylation of several transcription factors, which in turn regulate the expression of genes involved in DNA repair, cell cycle arrest, and apoptosis (18). Critically short dysfunctional telomeres trigger responses similar to those triggered by DNA damage, involving ATM and p53 (55). In concordance with these data, recent studies showed that many proteins that are involved in DNA repair and that are activated by ATM/ATR are overexpressed in the nuclei of senescent cells and form DNA damage foci at dysfunctional telomeres (8, 54) and intragenomic double-strand breaks (45). These proteins include phosphorylated H2AX (γ-H2AX), a common marker of cellular double-strand breaks that in turn promotes the assembly of several checkpoint and DNA repair factors (e.g., 53BP1, MDC1, and NBS1) at the site of DNA damage (17, 52). To explore whether the dysfunctional telomeres and double-strand breaks in senescent cells elicit a constitutive DNA damage signal irrespective of external factors, the localization and expression of these proteins (γ-H2AX, 53BP1, MDC1, and NBS1) in early- and late-passage HK1 cells under serial passage, serum starvation, and serum restimulation were monitored. In addition, a polyclonal antibody highly specific for phosphorylated substrates of ATM/ATR was used to monitor the activity status of this pathway. Immunofluorescence analysis revealed that most of the late-passage cells showed nuclear expression of the above proteins, which formed nuclear foci, as described previously (8, 45, 54). When the late-passage cells were transferred from serial passage (10% FBS) to serum starvation (0.1% FBS), the percentage of cells showing nuclear DNA damage foci was greatly reduced (Fig. 7). In parallel to our data on senescence signaling and phenotypic changes (see above), restimulation of serum-starved cells led to a rapid increase in the percentage of cells showing nuclear DNA damage foci (Fig. 7). In contrast to late-passage cells, a very small percentage of early-passage cells showed DNA damage foci, and there was no significant difference under the three culture conditions (Fig. 7D).

Inhibition of the MEK/MAPK pathway partially inhibits the amplification of senescence signaling and DNA damage responses induced by mitogen stimulation in cells with shortened telomeres. Treatment of cells with growth factors leads to the activation of MAPKs, also called extracellular signal-regulated kinases (ERKs), by the MAPK/ERK kinase (MEK). Members of the Ras family of oncoproteins activate this pathway in response to growth factor-mediated dimerization of tyrosine kinase receptors. Although necessary for normal cell proliferation, sustained overstimulation of the Ras/MEK/MAPK pathway induces premature senescence. Ras/MEK/MAPK-induced premature senescence is independent of telomere length and is characterized by the appearance of morphological and molecular markers similar to those seen in

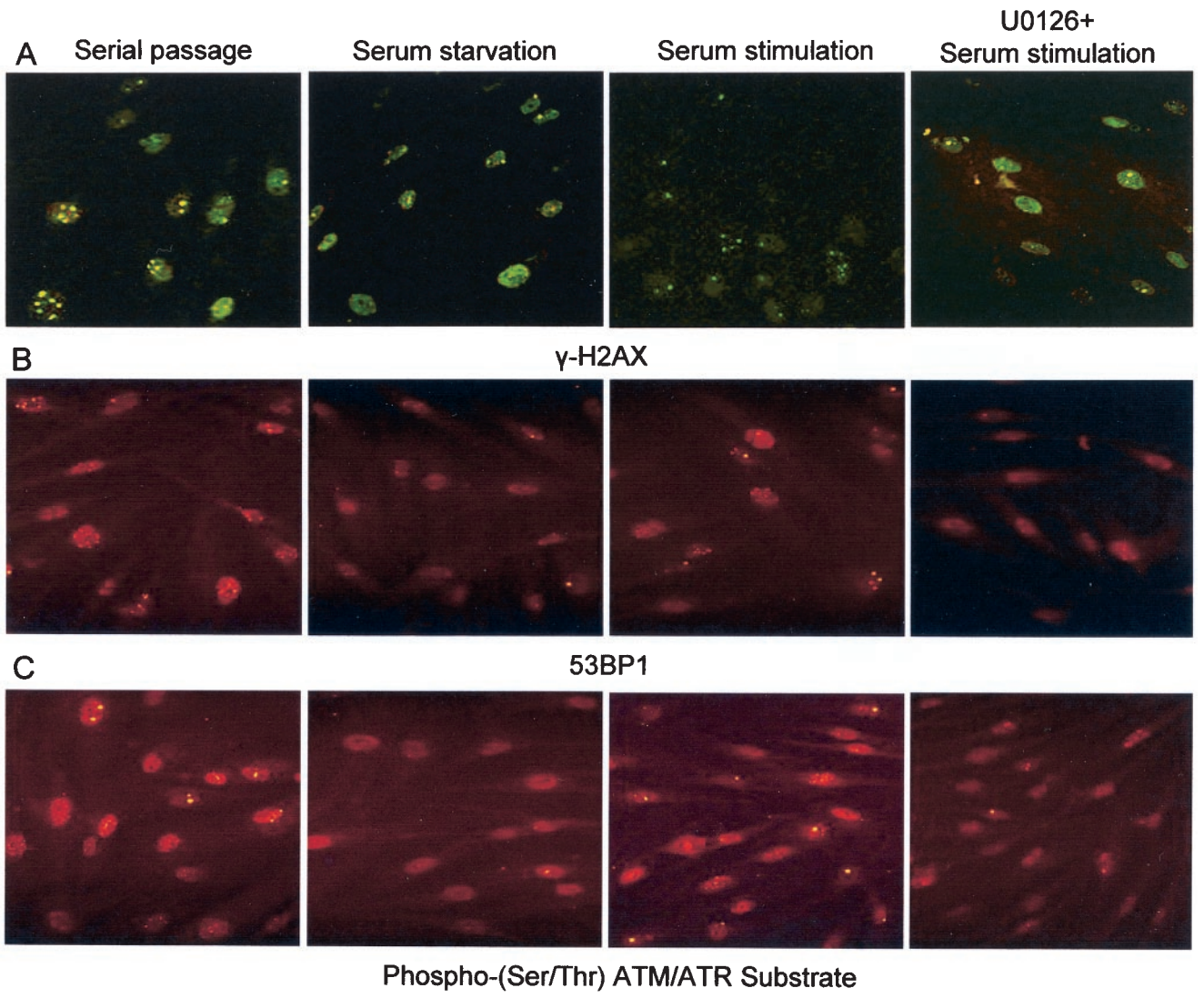
A
Serial passage
Serum starvation
Serum stimulation
U0126+
Serum stimulation
B
γ-H2AX
C
53BP1
Phospho-(Ser/Thr) ATM/ATR Substrate

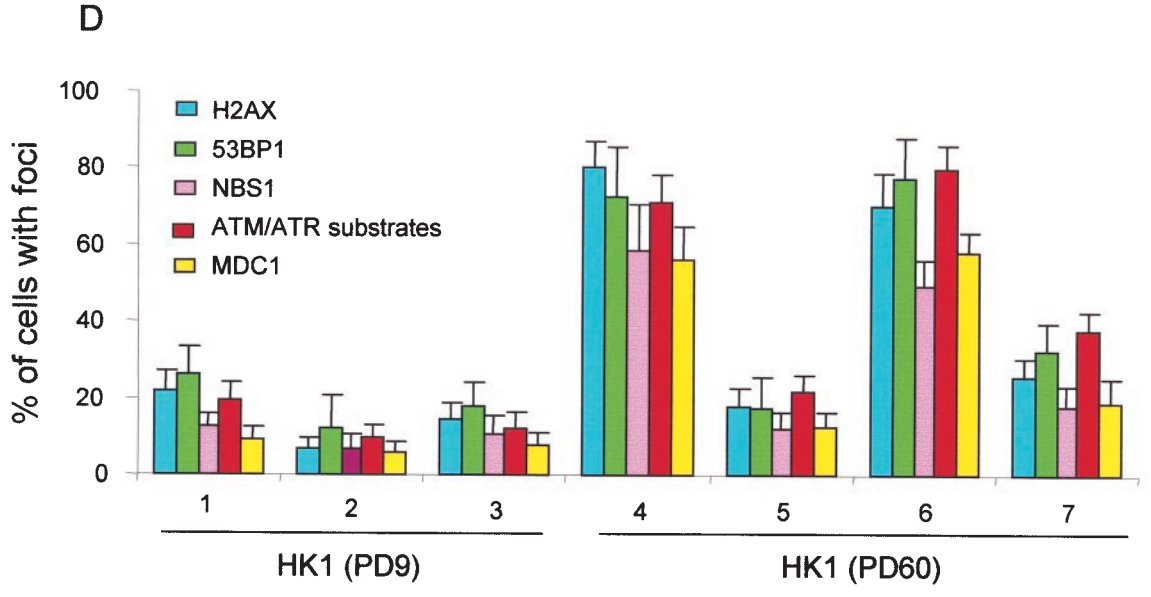
D
% of cells with foci
100
80
60
40
20
0
H2AX
53BP1
NBS1
ATM/ATR substrates
MDC1
1
2
3
4
5
6
7
HK1 (PD9)
HK1 (PD60)

replicative senescence (29, 46, 62). To test whether the same mitogenic pathway also plays a role in revealing DNA damage responses and senescence signaling during replicative senescence, two highly specific pharmacological inhibitors of MEK (PD098059 and U0126) were used to block this pathway (9, 16). When the cells were treated with PD098059 or U0126 1 h before serum stimulation of serum-starved late-passage IMR90 cells, the reappearance of senescence phenotypes (cell morphology and SA-β-Gal activity) (Fig. 2) was partially prevented (Fig. 8A to D). Similarly, the up-regulation of p21 and p16 in late-passage IMR90 cells in response to serum stimulation was significantly inhibited by the addition of PD098059 or U0126 (Fig. 8E to H). In addition, the reappearance of phosphorylated downstream targets of ATM/ATR and DNA damage response proteins in serum-restimulated senescent HK1 cells (data not shown for IMR90 cells) was strongly inhibited when the cells were treated with the MEK inhibitor U0126 1 h before serum stimulation (Fig. 7A to C and Fig. 7D, panel 7). Together, these data indicate that mitogen stimulation cooperates with telomere shortening through activation of the MEK/MAKP pathway to induce senescence signaling.

DISCUSSION

The present study shows that the phenotypes and signaling pathways of replicative senescence induced by telomere shortening become amplified to higher levels in cells that are stimulated to divide but that they operate at low, basal levels in the absence of a growth stimulus. We show that the morphological phenotypes and molecular markers of cellular senescence are dramatically diminished in mitogen-deprived cells and organs despite the prevalence of critically short telomeres. The senescence markers appear (or reappear) in response to mitogen stimulation both in vitro and in vivo, indicating that responses to telomere dysfunction are still intact. The mitogen-dependent induction of senescence phenotypes and signaling correlates with the appearance of nuclear DNA damage foci. The classical hypothesis of replicative senescence is that critically short telomeres at the chromosomal ends lose their capping function, resulting in the activation of DNA damage-like responses (55). In accordance with this hypothesis, recent studies have reported that senescent cells show an accumulation of DNA damage foci (45), some of which colocalize to dysfunctional telomeres (8, 54). The present study demonstrates that the activation of DNA damage responses in senescent cells, specifically, the activation and accumulation of proteins involved in DNA repair and checkpoint control downstream of ATM/ATR, is mitogen dependent. The rapid accumulation of DNA damage checkpoint and repair proteins in response to mitogen restimulation demonstrates that DNA damage signal transduction pathways can be activated instantaneously to prevent senescent cells from entering the cell cycle.

The present study shows that the activation of DNA damage responses and senescence signaling in response to mitogen stimulation occurs in part through the MEK/MAPK pathway, inducing premature senescence in response to sustained overstimulation of this pathway (29, 46, 62). Our data indicate that both senescence pathways (premature senescence and replicative senescence) are linked to each other. In line with this finding, previous studies showed that premature senescence and replicative senescence are indistinguishable in terms of morphological and molecular markers (46). Recently, it was shown that stress-induced MAPK 38 is overexpressed in both replicative senescence and premature senescence (26), indicating that there could be cross talk between mitogen stimulation and stress-induced MAPK 38.

A functional explanation for the mitogen dependence of replicative senescence is that low levels of cell cycle inhibitors are sufficient to counteract the actions of positive growth regulatory elements, which are either absent or present at very low levels under growth-depriving conditions (13, 48). Quiescent young and senescent human diploid fibroblasts (HDFs) express low levels of cyclin D1 and cyclin E. In the presence of serum stimulation, both the expression and the associated kinase activities of these cyclins increase during the mid- and late-G_1 phases, respectively, in young HDFs, leading to pRb phosphorylation (13, 48). In contrast to young HDFs, senescent HDFs, even though they contain abundant cyclin D-Cdk4/6 and cyclin E-Cdk2 complexes, lack cyclin E- and cyclin D-associated kinase activities due to increased inhibitory binding of p21 to these complexes rather than inhibitory phosphorylation of kinase activity (35, 51). In the present study, the enhanced expression of p21 in response to serum stimulation reflects the fact that a higher level of p21 is essential to inhibit the growth stimulatory effects of cyclin D-Cdk4/6 and cyclin E-Cdk2 complexes. The disappearance of morphological characteristics of senescent cells in response to serum deprivation correlates with diminished levels of expression of p21 and p16, indicating that the levels of expression of these genes may affect the morphological features of the cells. This explanation

FIG. 7. The appearance of nuclear DNA damage foci in senescent cells is mitogen dependent. (A to C) Representative images of late-passage (PD60) HK1 cells under the indicated culture conditions and probed with anti-γ-H2AX antibody followed by FITC-conjugated secondary antibody (A), anti-53BP1 antibody followed by CY_3-conjugated secondary antibody (B), and phospho-(Ser/Thr) ATM/ATR substrate antibody followed by CY_3-conjugated secondary antibody (C). The images were taken with a fluorescence microscope (magnification, ca. ×37). (D) Histogram showing the percentage of cells that stained positively with the indicated antibodies in early-passage (PD9) HK1 cells under serial passage (10% FBS) (panel 1), serum starvation (0.1% FBS) (panel 2), and serum restimulation (10% FBS) (panel 3) and in late-passage (PD60) HK1 cells under serial passage (10% FBS) (panel 4), serum starvation (0.1% FBS) (panel 5), and serum restimulation (10% FBS) (panel 6). Relatively few early-passage cells compared to late-passage cells showed nuclear foci in response to all of the antibodies tested. Interestingly, the high percentage of late-passage cells that showed nuclear DNA damage foci was greatly reduced in response to serum starvation but rapidly reinduced in response to restimulation with 10% FBS. The reinduction of DNA damage foci by serum restimulation of late-passage cells was not seen when the cells were treated with MEK inhibitor U0126, which inhibits the MEK/MAPK pathway (panel 7). The inhibitor was applied 1 h before serum stimulation. In response to serum starvation or drug treatment, not only did the percentage of cells showing nuclear DNA damage foci decrease but also the number of foci per nucleus decreased. Histogram data are presented as means and standard deviations.

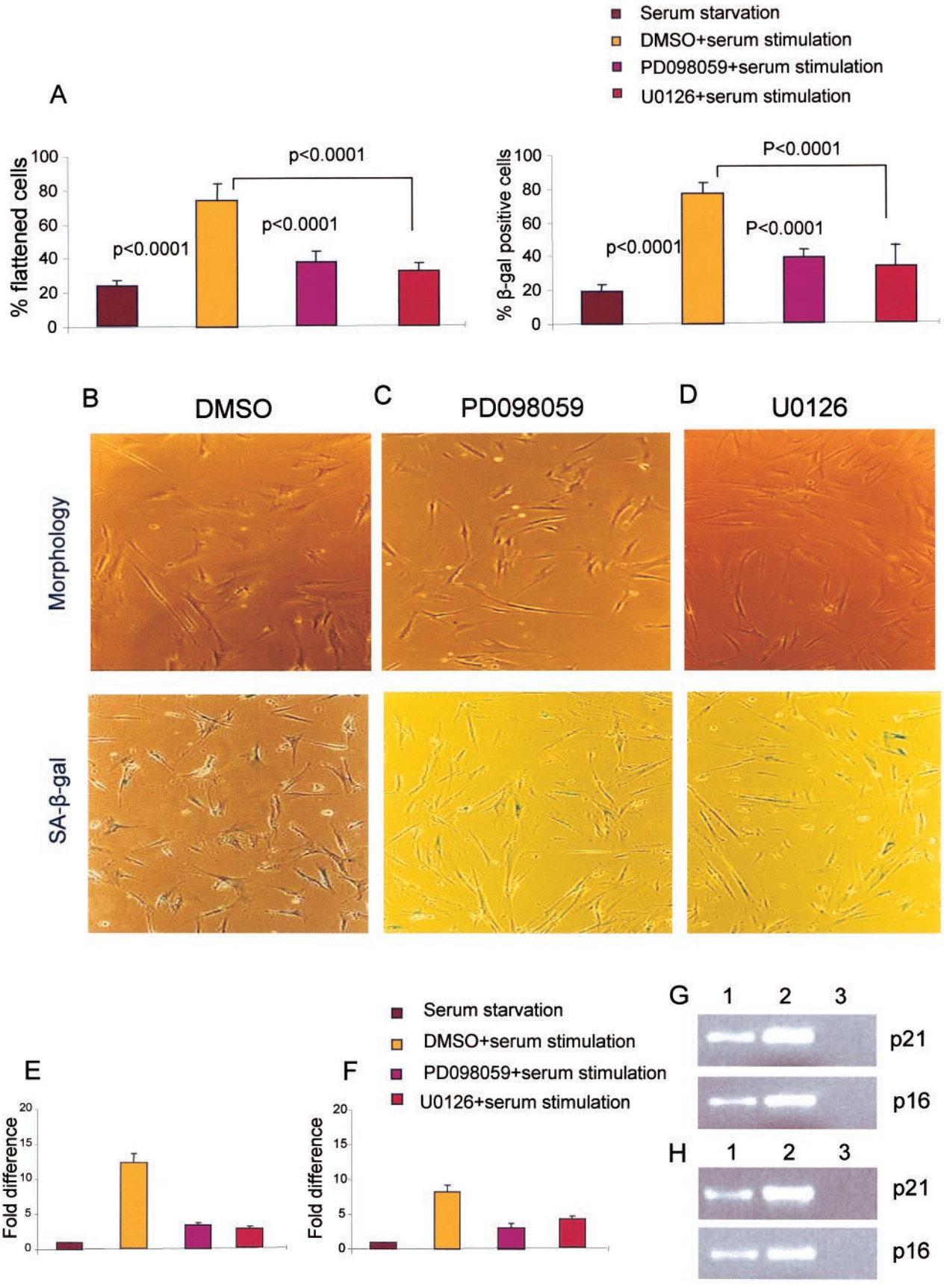
Serum starvation
DMSO+serum stimulation
PD098059+serum stimulation
U0126+serum stimulation
A
% flattened cells
p<0.0001
p<0.0001
p<0.0001
% β-gal positive cells
P<0.0001
P<0.0001
p<0.0001
B
DMSO
C
PD098059
D
U0126
Morphology
SA-β-gal
E
Fold difference
F
Fold difference
G
1 2 3
p21
p16
H
1 2 3
p21
p16

FIG. 8. (A) Histogram of the percentage of cells showing senescent morphology or positive SA-β-Gal staining in late-passage IMR90 cells 120 h after serum starvation and 24 h after serum stimulation following treatment with dimethyl sulfoxide (DMSO) or MEK inhibitors PD098059 and U0126 1 h before stimulation. (B to D) Representative images showing senescent morphology and SA-β-Gal activity in late-passage IMR90 cells in response to serum stimulation for 24 h following the addition of DMSO (B) and MEK inhibitors PD098059 (C) and U0126 (D). (E) Fold difference in p21 expression in late-passage IMR90 cells 120 h after serum starvation and 24 h after serum stimulation following the addition of DMSO or MEK inhibitors PD098059 and U0126. (F) Fold difference in p16 expression in late-passage IMR90 cells 120 h after serum starvation and 24 h after serum stimulation following the addition of DMSO or MEK inhibitors PD098059 and U0126. (G) Representative gel electrophoresis image showing the levels of expression of p21 and p16 obtained by analysis of 10 μl of the RT-PCR product after 22 PCR cycles in the presence of PD098059. Lanes: 1, late-passage IMR90 cells under serum stimulation plus PD098059; 2, late-passage IMR90 cells under serum stimulation plus DMSO; 3, nontemplate control. (H) Representative gel electrophoresis image showing the levels of expression of p21 and p16 obtained by analysis of 10 μl of the RT-PCR product after 22 PCR cycles in the presence of U0126. Lanes: 1, late-passage IMR90 cells under serum stimulation plus U0126; 2, late-passage IMR90 cells under serum stimulation plus DMSO; 3, nontemplate control. Histogram data are presented as means and standard deviations.

is in accord with previous reports indicating that the induced expression of either p21 or p16 alone is sufficient to induce senescence with all of the morphological markers of senescence, including flattened morphology and SA-β-Gal activity (14, 22, 33), and that the inhibition of p21 and p16 leads to normal cell cycle progression and extension of the life span with no signs of senescence (7, 12, 30). In the present study, the disappearance and reappearance of morphological features of senescence (flattened cells and SA-β-Gal activity) in response to serum starvation and serum stimulation correlate with the levels of expression of p21 and p16.

The results of our study will have an impact on future analysis of the senescence pathway and may help to identify the initial responses to telomere shortening leading to cell cycle arrest and senescence. Regarding the role of replicative senescence in vivo, our findings indicate the need to monitor cell cycle activity in order to analyze the prevalence and consequences of senescence in different organs and tissues often containing large fractions of cells in the G_0 phase of the cell cycle.

ACKNOWLEDGMENTS

We thank H. Sundblat and N. P. Malek for critical reading of the manuscript and valuble discussions. We thank Stephen P. Jackson for providing antibody MDC1.

K.L.R is supported by the Deutsche Forschungsgemeinschaft (Emmy-Noether-Programm: Ru 745/2-1 and KFO119) and by a grant from the Deutsche Krebshilfe e.V. (10-1809-Ru1). W.C.H. is supported in part by a Doris Duke Charitable Foundation clinical scientist development award and a Kimmel Scholar award.

REFERENCES

1. **Albrecht, J. H., A. H. Meyer, and M. Y. Hu.** 1997. Regulation of cyclin-dependent kinase inhibitor p21(WAF1/Cip1/Sdi1) gene expression in hepatic regeneration. Hepatology **25:**557–563.
2. **Alcorta, D. A., Y. Xiong, G. Hannon, D. Beach, and J. C. Barrett.** 1996. Involvement of the cyclin-dependent kinase inhibitor p16 (INK4a) in replicative senescence of normal human fibroblasts. Proc. Natl. Acad. Sci. USA **93:**13742–13747.
3. **Allsopp, R. C., and C. B. Harley.** 1995. Evidence for a critical telomere length in senescent human fibroblasts. Exp. Cell Res. **219:**130–136.
4. **Balagurumoorthy, P., S. K. Brahmachari, D. Mohanty, M. Bansal, and V. Sasisekharan.** 1992. Hairpin and parallel quartet structures for telomeric sequences. Nucleic Acids Res. **20:**4061–4067.
5. **Bayreuther, K., H. P. Rodemann, R. Hommel, K. Dittmann, M. Albiez, and P. I. Francz.** 1998. Human skin fibroblasts in vitro differentiate along a terminal cell lineage. Proc. Natl. Acad. Sci. USA **85:**5112–5116.
6. **Blasco, M. A., H. W. Lee, M. P. Hande, E. Samper, P. M. Lansdorp, R. A. DePinho, and C. W. Greider.** 1997. Telomere shortening and tumor formation by mouse cells lacking telomerase RNA. Cell **91:**25–34.
7. **Brown, J. P., W. Wei, and J. M. Sedivy.** 1997. Bypass of senescence after disruption of p21CIP1/WAF1 gene in normal diploid human fibroblasts. Science **277:**831–834.
8. **d'Adda di Fagagna, F., P. M. Reaper, L. Clay-Farrace, H. Fiegler, P. Carr, T. Von Zglinicki, G. Saretzki, N. P. Carter, and S. P. Jackson.** 2003. A DNA damage checkpoint response in telomere-initiated senescence. Nature **426:**194–198.
9. **Dadley, D. T., L. Pang, S. J. Decker, A. J. Bridges, and A. R. Saltiel.** 1995. A synthetic inhibitor of the mitogen-activated protein kinase cascade. Proc. Natl. Acad. Sci. USA **92:**7686–7689.
10. **Dimri, G. P., X. Lee, G. Basile, M. Acosta, G. Scott, C. Roskelley, E. E. Medrano, M. Linskens, I. Rubelj, O. Pereira-Smith, M. Peacocke, and J. Campisi.** 1995. A biomarker that identifies senescent human cells in culture and in aging skin in vivo. Proc. Natl. Acad. Sci. USA **92:**9363–9367.
11. **Dimri, G. P., K. Itahana, M. Acosta, and J. Campisi.** 2000. Regulation of a senescence checkpoint response by the E2F1 transcription factor and p14(ARF) tumor suppressor. Mol. Cell. Biol. **20:**273–285.
12. **Duan, J., Z. Zhang, and T. Tong.** 2001. Senescence delay of human diploid fibroblast induced by anti-sense p16INK4a expression. J. Biol. Chem. **276:**48325–48331.
13. **Dulic, V., L. F. Drullinger, E. Lees, S. I. Reed, and G. H. Stein.** 1993. Altered regulation of G1 cyclins in senescent human diploid fibroblasts: accumulation of inactive cyclin E-Cdk2 and cyclin D1-Cdk2 complexes. Proc. Natl. Acad. Sci. USA **90:**11034–11038.
14. **Fang, L., M. Igarashi, J. Leung, M. M. Sugrue, S. W. Lee, and S. A. Aaronson.** 1999. p21Waf1/Cip1/Sdi1 induces permanent growth arrest with markers of replicative senescence in human tumor cells lacking functional p53. Oncogene **18:**2789–2797.
15. **Fausto, N.** 2000. Liver regeneration. J. Hepatol. **32**(Suppl. 1)**:**19–31.
16. **Favata, M. F., K. Y. Horiuchi, E. J. Manos, A. J. Daulerio, D. A. Stradley, W. S. Feeser, D. E. Van Dyk, W. J. Pitts, R. A. Earl, F. Hobbs, R. A. Copeland, R. L. Magolda, P. A. Scherle, and J. M. Trzaskos.** 1998. Identification of a novel inhibitor of mitogen-activated protein kinase kinase. J. Biol. Chem. **273:**18623–18632.
17. **Fernandez-Capetillo, O., H. T. Chen, A. Celeste, I. Ward, P. J. Romanienko, J. C. Morales, K. Naka, Z. Xia, R. D. Camerini-Otero, N. Motoyama, P. B. Carpenter, W. M. Bonner, J. Chen, and A. Nussenzweig.** 2002. DNA damage-induced G2-M checkpoint activation by histone H2AX and 53BP1. Nat. Cell Biol. **4:**993–997.
18. **Goodarzi, A. A., W. D. Block, and S. P. Lees-Miller.** 2003. The role of ATM and ATR in DNA damage-induced cell cycle control. Prog. Cell Cycle Res. **5:**393–411.
19. **Griffith, J. D., L. Comeau, S. Rosenfield, R. M. Stansel, A. Bianchi, H. Moss, and T. de Lange.** 1999. Mammalian telomeres end in a large duplex loop. Cell **97:**503–514.
20. **Hara, E., R. Smith, D. Parry, H. Tahara, S. Stone, and G. Peters.** 1996. Regulation of $p16^{CDKN2}$ expression and its implications for cell immortalization and senescence. Mol. Cell. Biol. **16:**859–867.
21. **Harley, C. B., A. B. Futcher, and C. W. Greider.** 1990. Telomeres shorten during ageing of human fibroblasts. Nature **345:**458–460.
22. **Harper, J. W., S. J. Elledge, K. Keyomarsi, B. Dynlacht, L. H. Tsai, P. Zhang, S. Dobrowolski, C. Bai, L. Connell-Crowley, and E. Swindell.** 1995. Inhibition of cyclin-dependent kinases by p21. Mol. Biol. Cell **6:**387–400.
23. **Hayflick, L.** 1965. The limited in vitro life time of diploid cell strains. Exp. Cell Res. **37:**614–636.
24. **Herrera, E., E. Samper, J. Martin-Caballero, J. M. Flores, H. W. Lee, and M. A. Blasco.** 1999. Disease states associated with telomerase deficiency appear earlier in mice with short telomeres. EMBO J. **18:**2950–2960.
25. **Itahana, K., Y. Zou, Y. Itahana, J. L. Martinez, C. Beausejour, J. J. Jacobs, M. Van Lohuizen, V. Band, J. Campisi, and G. P. Dimri.** 2003. Control of the replicative life span of human fibroblasts by p16 and the polycomb protein Bmi-1. Mol. Cell. Biol. **23:**389–401.
26. **Iwasa, H., J. Han, and F. Ishikawa.** 2003. Mitogen-activated protein kinase p38 defines the common senescence-signalling pathway. Genes Cells **8:**131–144.

27. **Kim, H., S. You, J. Farris, B. W. Kong, S. A. Christman, L. K. Foster, and D. N. Foster.** 2002. Expression profiles of p53-, p16(INK4a)-, and telomere-regulating genes in replicative senescent primary human, mouse, and chicken fibroblast cells. Exp. Cell Res. **272:**199–208.
28. **Lee, H. W., M. A. Blasco, G. J. Gottlieb, J. W. Horner II, C. W. Greider, and R. A. DePinho.** 1998. Essential role of mouse telomerase in highly proliferative organs. Nature **392:**569–574.
29. **Lin, A. W., M. Barradas, J. C. Stone, L.van Aelst, M. Serrano, and S. W. Lowe.** 1998. Premature senescence involving p53 and p16 is activated in response to constitutive MEK/MAPK mitogenic signaling. Genes Dev. **12:** 3008–3019.
30. **Macip, S., M. Igarashi, L. Fang, A. Chen, Z. Q. Pan, S. W. Lee, and S. A. Aaronson.** 2002. Inhibition of p21-mediated ROS accumulation can rescue p21-induced senescence. EMBO J. **21:**2180–2188.
31. **Masutomi, K., E. Y. Yu, S. Khurts, I. Ben-Porath, J. L. Currier, G. B. Metz, M. W. Brooks, S. Kaneko, S. Murakami, J. A. DeCaprio, R. A. Weinberg, S. A. Stewart, and W. C. Hahn.** 2003. Telomerase maintains telomere structure in normal human cells. Cell **114:**241–253.
32. **Matuoka, K., and K. Y. Chen.** 2002. Telomerase positive human diploid fibroblasts are resistant to replicative senescence but not premature senescence induced by chemical reagents. Biogerontology **3:**365–372.
33. **McConnell, B. B., M. Starborg, S. Brookes, and G. Peters.** 1998. Inhibitors of cyclin-dependent kinases induce features of replicative senescence in early passage human diploid fibroblasts. Curr. Biol. **8:**351–354.
34. **Nicholas, R., N. R. Forsyth, A. P. Evans, J. W. Shay, and W. E. Wright.** Aging Cell, in press.
35. **Noda, A., Y. Ning, S. F. Venable, S. O. Pereira, and J. R. Smith.** 1994. Cloning of senescent cell-derived inhibitors of DNA synthesis using an expression screen. Exp. Cell Res. **211:**90–98.
36. **Ouellette, M. M., D. L. Aisner, I. Savre-Train, W. E. Wright, and J. W. Shay.** 1999. Telomerase activity does not always imply telomere maintenance. Biochem. Biophys. Res. Commun. **254:**795–803.
37. **Pang, J. H., and K. Y. Chen.** 1994. Global change of gene expression at late G1/S boundary may occur in human IMR-90 diploid fibroblasts during senescence. J. Cell Physiol. **160:**531–538.
38. **Paradis, V., N. Youssef, D. Dargere, N. Ba, F. Bonvoust, J. Deschatrette, and P. Bedossa.** 2001. Replicative senescence in normal liver, chronic hepatitis C, and hepatocellular carcinomas. Hum. Pathol. **32:**327–332.
39. **Parrinello, S., E. Samper, A. Krtolica, J. Goldstein, S. Melov, and J. Campisi.** 2003. Oxygen sensitivity severely limits the replicative lifespan of murine fibroblasts. Nat. Cell Biol. **5:**741–747.
40. **Pignolo, R. J., B. G. Martin, J. H. Horton, A. N. Kalbach, and V. J. Cristofalo.** 1998. The pathway of cell senescence: WI-38 cells arrest in late G1 and are unable to traverse the cell cycle from a true G0 state. Exp. Gerontol. **33:**67–80.
41. **Rittling, S. R., K. M. Brooks, V. J. Cristofalo, and R. Baserga.** 1986. Expression of cell cycle dependent genes in young and senescent WI38 fibroblasts. Proc. Natl. Acad. Sci. USA **83:**3316–3320.
42. **Rudolph, K. L., S. Chang, H. W. Lee, M. Blasco, G. J. Gottlieb, C. Greider, and R. A. DePinho.** 1999. Longevity, stress response, and cancer in aging telomerase-deficient mice. Cell **96:**701–712.
43. **Rudolph, K. L., S. Chang, M. Millard, N. Schreiber-Agus, and R. A. DePinho.** 2000. Inhibition of experimental liver cirrhosis in mice by telomerase gene delivery. Science **287:**1253–1258.
44. **Satyanarayana, A., S. U. Wiemann, J. Buer, J. Lauber, K. E. Dittmar, T. Wustefeld, M. A. Blasco, M. P. Manns, and K. L. Rudolph.** 2003. Telomere shortening impairs organ regeneration by inhibiting cell cycle re-entry of a subpopulation of cells. EMBO J. **22:**4003–4013.
45. **Sedelnikova, O. A., I. Horikawa, D. B. Zimonjic, N. C. Popescu, W. M. Bonner, and J. C. Barrett.** 2004. Senescing human cells and ageing mice accumulate DNA lesions with unrepairable double-strand breaks. Nat. Cell Biol. **6:**168–170.
46. **Serrano, M., A. W. Lin, M. E. McCurrach, D. Beach, and S. W. Lowe.** 1997. Oncogenic ras provokes premature cell senescence associated with accumulation of p53 and p16INK4a. Cell **88:**593–602.
47. **Seshadri, T., and J. Campisi.** 1990. c-fos repression and an altered genetic program in senescent human fibroblasts. Science **247:**205–209.
48. **Sherr, C. J.** 1994. G1 phase progression: cycling on cue. Cell **79:**551–555.
49. **Smogorzewska, A., and T. de Lange.** 2002. Different telomere damage signaling pathways in human and mouse cells. EMBO J. **21:**4338–4348.
50. **Stein, G. H., M. Beeson, and L. Gordon.** 1990. Failure to phosphorylate the retinoblastoma gene product in senescent human fibroblasts. Science **249:** 666–669.
51. **Stein, G. H., L. F. Drullinger, A. Soulard, and V. Dulic.** 1999. Differential roles for cyclin-dependent kinase inhibitors p21 and p16 in the mechanisms of senescence and differentiation in human fibroblasts. Mol. Cell. Biol. **19:** 2109–2117.
52. **Stewart, G. S., B. Wang, C. R. Bignell, A. M. Taylor, and S. J. Elledge.** 2003. MDC1 is a mediator of the mammalian DNA damage checkpoint. Nature **421:**961–966.
53. **Stewart, S. A., I. Ben-Porath, V. J. Carey, B. F. O'Connor, W. C. Hahn, and R. A. Weinberg.** 2003. Erosion of the telomeric single-strand overhang at replicative senescence. Nat. Genet. **33:**492–496.
54. **Takai, H., A. Smogorzewska, and T. de Lange.** 2003. DNA damage foci at dysfunctional telomeres. Curr. Biol. **13:**1549–1556.
55. **Vaziri, H., and S. Benchimol.** 1996. From telomere loss to p53 induction and activation of a DNA-damage pathway at senescence: the telomere loss/DNA damage model of cell aging. Exp. Gerontol. **31:**295–301.
56. **Veelken, H., H. Jesuiter, A. Mackensen, P. Kulmburg, J. Schultze, F. Rosenthal, R. Mertelsmann, and A. Lindemann.** 1994. Primary fibroblasts from human adults as target cells for ex vivo transfection and gene therapy. Hum. Gene Ther. **5:**1203–1210.
57. **von Zglinicki, T.** 2002. Oxidative stress shortens telomeres. Trends Biochem. Sci. **27:**339–344.
58. **Wei, W., R. M. Hemmer, and J. M. Sedivy.** 2001. Role of p14(ARF) in replicative and induced senescence of human fibroblasts. Mol. Cell. Biol. **21:**6748–6757.
59. **Weinberg, R. A.** 1995. The retinoblastoma protein and cell cycle control. Cell **81:**323–330.
60. **Wiemann, S. U., A. Satyanarayana, M. Tsahuridu, H. L. Tillmann, L. Zender, J. Klempnauer, P. Flemming, S. Franco, M. A. Blasco, M. P. Manns, and K. L. Rudolph.** 2002. Hepatocyte telomere shortening and senescence are general markers of human liver cirrhosis. FASEB J. **16:**935–942.
61. **Wright, W. E., and J. W. Shay.** 1992. Re-expression of senescent markers in deinduced reversibly immortalized cells. Exp. Gerontol. **27:**383–389.
62. **Zhu, J., D. Woods, M. McMahon, and J. M. Bishop.** 1998. Senescence of human fibroblasts induced by oncogenic Raf. Genes Dev. **12:**2997–3007.
63.. **Zimmermann, S., S. Glaser, R. Ketteler, C. F. Waller, V. Klingmüller, and U. M. Martens.** Effects of telomerase modulation in human hematopoietic progenitor cells. Stem Cells, in press.